Journal of Luminescence 222 (2020) 117101

Contents lists available at ScienceDirect

Journal of Luminescence

journal homepage: http://www.elsevier.com/locate/jlumin

Engineering near-infrared emitting scintillators with efficient $Eu^{2+} \rightarrow Sm^{2+}$ energy transfer

W. Wolszczak [a,*], K.W. Krämer [b], P. Dorenbos [a]

[a] Faculty of Applied Sciences, Department of Radiation Science and Technology, Section Luminescence Materials, Delft University of Technology, Mekelweg 15, 2629, JB Delft, the Netherlands

[b] Department of Chemistry and Biochemistry, Bern University, Freiestrasse 3, CH-3012, Bern, Switzerland

A B S T R A C T

Recently, we proposed a concept for a new class of near infrared (NIR) scintillators by employing efficient $Eu^{2+} \rightarrow Sm^{2+}$ energy transfer. In this article we investigate the optical spectroscopy of Sm^{2+} in BaBrI, $CsSrI_3$, and $CsBa_2I_5$ halide hosts. A criterion was derived for fast Sm^{2+} 5d → 4f emission and a list of new potential NIR scintillators is proposed.

1. Introduction

Scintillators are important materials for the detection of ionizing radiation [1–3]. They can absorb a high energy particle and down-convert its energy into a short pulse of (visible) light. The linear dependence between the absorbed energy and the number of emitted photons is the basis of gamma spectroscopy. Scintillators are used in numerous applications like medical imaging [4], homeland security [5], space exploration [6–8], or high energy physics [9,10]. High energy resolution is one of the important properties vital for these applications.

Europium-doped halide scintillators (SrI_2:Eu^{2+} [11], BaBrI:Eu^{2+} [12], $CsBa_2I_5$:Eu^{2+} [13]) are among the ones that offer the highest energy resolution and light yield [14]. One of the reasons is that Eu^{2+} can be incorporated in high concentration without concentration quenching. However, the re-absorption of Eu^{2+} luminescence by other Eu^{2+} atoms (self-absorption) is detrimental to the scintillation process in large crystals required for γ-spectroscopy. It affects decay time, light yield, and energy resolution [11]. We proposed a solution to that problem by adding a co-dopant at low concentration which absorbs Eu^{2+} emission and re-emits it at a longer wavelength. The idea of Sm^{2+} codoping has been evidenced recently by us in SrI_2:Eu,Sm [15] and $CsBa_2I_5$:Eu,Sm [16]. Especially for $CsBa_2I_5$ we observed surprisingly good NIR scintillation performance, and an energy resolution of 3.2% was achieved for 662 keV gamma ray detection with an Avalanche Photodiode (APD) readout. Besides limiting the self-absorption, shifting the emission wavelength to the near infrared NIR can be a way to an energy resolution better than 2% [16].

In this article we explore the potential of parity-allowed 5d → 4f transitions of Sm^{2+} for developing new scintillators with efficient energy transfer between europium and samarium. Three halide host lattices were chosen with high energy resolution and light yield when doped with europium. We present the spectroscopic characterization of BaBrI:Eu^{2+},Sm^{2+}, $CsBa_2I_5$:Eu^{2+},Sm^{2+}, and $CsSrI_3$:Eu^{2+},Sm^{2+} and derive a criterion for fast Sm^{2+} 5d → 4f emission in a host lattice.

2. Sample synthesis and crystal growth

BaBrI:Eu^{2+},Sm^{2+} was synthesized from stoichiometric amounts of the binary halides $BaBr_2$, BaI_2, EuI_2, and SmI_2. $BaBr_2$ and BaI_2 were prepared from $BaCO_3$ (Alfa Aesar, 4N7). The carbonate was dissolved in concentrated hydrobromic (Merck, suprapur 47%) or hydroiodic acid (Merck, suprapur 57%), respectively. The product was dried up on a sandbath, heated to 450 °C in vacuum ($< 10^{-3}$ mbar), and purified by Bridgman crystal growth in a glassy carbon ampoule. EuI_2 was synthesized from Eu metal (Stanford materials, 4 N) and iodine (Merck, p. a.). The starting materials were sealed in a silica ampoule under vacuum. The ampoule was heated in a tube furnace keeping the colder end at about 100 °C to avoid an overpressure. The metal was slowly heated and kept at 500 °C until the iodine had reacted completely. EuI_2 was sublimed for purification in a tantalum ampoule under vacuum at 1000 °C. SmI_3 was prepared in a similar way from Sm metal (Alfa, 3 N). The ampoule was heated to 400 °C and SmI_3 was sublimed at 800 °C in a silica ampoule. SmI_2 was obtained by reacting SmI_3 with Sm in a tantalum ampoule at 900 °C for 2 days. The tantalum ampoule was sealed by He-arc welding and encapsulated into a silica ampoule under vacuum.

* Corresponding author.
E-mail address: w.w.wolszczak@tudelft.nl (W. Wolszczak).

https://doi.org/10.1016/j.jlumin.2020.117101
Received 29 August 2019; Received in revised form 31 January 2020; Accepted 5 February 2020
Available online 12 February 2020
0022-2313/Published by Elsevier B.V. This is an open access article under the CC BY license (http://creativecommons.org/licenses/by/4.0/).

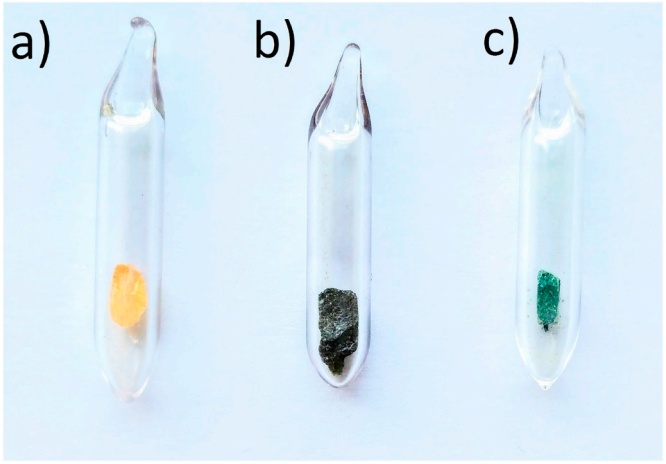

Fig. 1. The studied samples were encapsulated in fused silica ampules: a) BaBrI:5%Eu^{2+},0.5%Sm^{2+}; b) $CsBa_2I_5$:2%Eu^{2+},1%Sm^{2+}; and c) $CsSrI_3$:2% Eu^{2+},1%Sm^{2+}.

Crystals of BaBrI:Eu^{2+},Sm^{2+} were grown by the Bridgman technique using a vertical, static ampoule with seed selection tip and a moving furnace. The starting materials were sealed in a silica ampoule under vacuum and heated to 780 °C for 1 day. BaBrI melts congruently at 770 °C. Then the furnace was slowly moved up by a controlled stepper motor with 0.6 mm/h cooling the crystal to room temperature within about 10 days. The ampoules were opened in a glove box (MBraun, Graching, D) equipped with a microscope and with water and oxygen values < 0.1 ppm. Crystals were cleaved from the boule and pieces of about 5 mm size were sealed in small silica ampoules for further spectroscopic characterization. The phase purity of the product was verified by powder X-ray diffraction on a Stoe Stadip diffractometer in Bragg-Brentano (reflection) geometry with $CuK_{\alpha 1}$ radiation from a curved (101) α-SiO_2 monochromator and a linear position sensitive detector. BaBrI adopts the $PbCl_2$ crystal structure (orthorhombic, Pnma, no. 62) as its parent compounds $BaBr_2$ and BaI_2 [17]. Since starting materials and products are hygroscopic all handling was done under strictly dry conditions in glove boxes or sealed containers.

$CsSrI_3$:Eu^{2+},Sm^{2+} was synthesized from stoichiometric amounts of the binary halides CsI, SrI_2, EuI_2, and SmI_2. CsI (Merck, suprapur) was dried in vacuum at 250 °C. SrI_2 was synthesized from $SrCO_3$ (Alfa Aesar, 4N4) as described above for BaI_2.

Crystals of $CsSrI_3$:Eu,Sm were grown by the Bridgman technique. The starting materials were sealed in a silica ampoule under vacuum and heated to 660 °C for 1 day. $CsSrI_3$ melts congruently at 650 °C. Then the furnace was slowly moved up by a controlled stepper motor with 0.6 mm/h cooling the crystal to room temperature within about 10 days. The ampoules were opened in a glove box. Crystals were cleaved from the boule and pieces of about 5 mm size were sealed in small silica ampoules for further spectroscopic characterization. The phase purity of the product was verified by powder X-ray diffraction. $CsSrI_3$ crystallizes in the stuffed $PuBr_3$ structure (orthorhombic, Cmcm, no. 63) [18]. Since starting materials and products are hygroscopic all handling was done under strictly dry conditions in glove boxes or sealed containers.

Synthesis and crystal growth of $CsBa_2I_5$:Eu^{2+},Sm^{2+} sample has been described previously in Ref. [16]. Fig. 1 shows the studied single crystal samples encapsulated in fused silica ampules. Dopant concentrations are expressed in mol% and refer to the dopant concentration in the melt. As this is pioneering research in a new field of materials and dopants for scintillator application, we selected relatively high doping concentrations to facilitate energy transfer. The chosen concentrations are somewhat arbitrary because we do not know what the optimal will be.

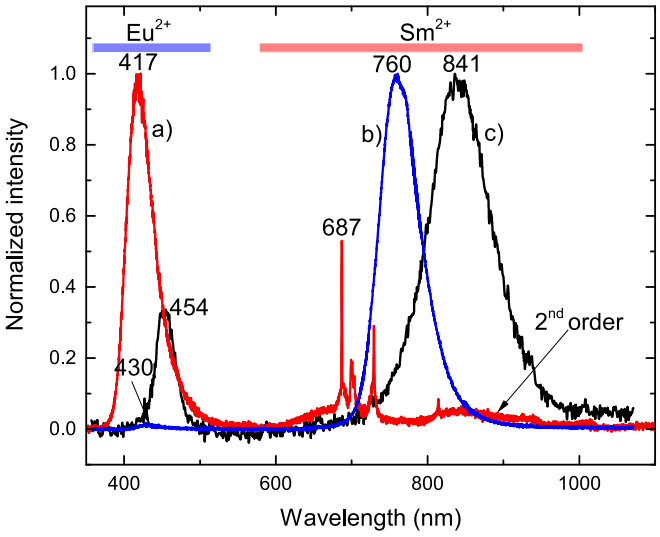

Fig. 2. Room temperature emission spectra of a) BaBrI:5%Eu^{2+},0.5%Sm^{2+} ($\lambda_{exc.}$ = 350 nm), b) $CsBa_2I_5$:2%Eu^{2+},1%Sm^{2+} ($\lambda_{exc.}$ = 360 nm), and c) $CsSrI_3$:2%Eu^{2+},1%Sm^{2+} ($\lambda_{exc.}$ = 360 nm) excited by a xenon lamp and measured with a 300 nm blazed monochromator coupled to a CCD detector. The spectra are not corrected for the monochromator and detector efficiencies.

3. Experimental methods

Photoluminescence excitation and emission measurements at room temperature were measured with a Horiba Scientific QuantaMaster fluorometer with single grating monochromators. Time and temperature resolved measurements were made with an Ekspla NT230 Optical Parametric Oscillator (OPO) laser or Newport 66921 xenon lamp excitation in combination with a Horiba Gemini 180 monochromator. The emission of the sample was dispersed with a Princeton Instruments Acton SP 2300 monochromator and detected with a Hamamatsu R7600U-20 (300–920 nm) or R7600U-03 (185–650 nm) photomultiplier tube (PMT), or a Hamamatsu C9100-13 electron multiplier CCD camera. Time resolved spectra were recorded using a CAEN DT5724 or DT5730 digitizer connected to one of the PMTs and controlled by home made software. The sample was placed in a Janis Research VPF-700 cryostat and its' temperature stabilized with a LakeShore 331 controller. A closed cycle helium refrigerator has been used for low temperature measurements.

4. Results

4.1. Optical spectroscopy of Sm^{2+}

Fig. 2 shows photoluminescence emission spectra of BaBrI:5% Eu^{2+},0.5%Sm^{2+}, $CsBa_2I_5$:2%Eu^{2+},1%Sm^{2+}, and $CsSrI_3$:2%Eu^{2+},1% Sm^{2+} measured at room temperature. The typical Eu^{2+} and Sm^{2+} 5d-4f emission ranges are marked at the top. The Eu^{2+} emission in all three studied hosts is characterized by a single broad peak ascribed to the spin allowed 5d-4f transitions. The Eu^{2+} peak red-shifts with change of the host in the sequence from BaBrI (417 nm), $CsBa_2I_5$ (430 nm), to $CsSrI_3$ (454 nm). Similar red-shift is observed for Sm^{2+} emission, however, the Sm^{2+} emission in BaBrI is more complex; it is characterized by five sharp 4f-4f transition lines on top of a weak broad 5d-4f emission band around 700 nm. The second order dispersion of the europium peak is present between 800 and 1000 nm in the BaBrI spectrum. The Sm^{2+} 5d-4f emissions in $CsBa_2I_5$ and $CsSrI_3$ are observed at 760 and 841 nm, respectively.

Fig. 3 shows photoluminescence emission and excitation spectra of europium and samarium ions in BaBrI:5%Eu^{2+},0.5%Sm^{2+} measured at room temperature and 13 K. The 729 nm Sm^{2+} emission wavelength was

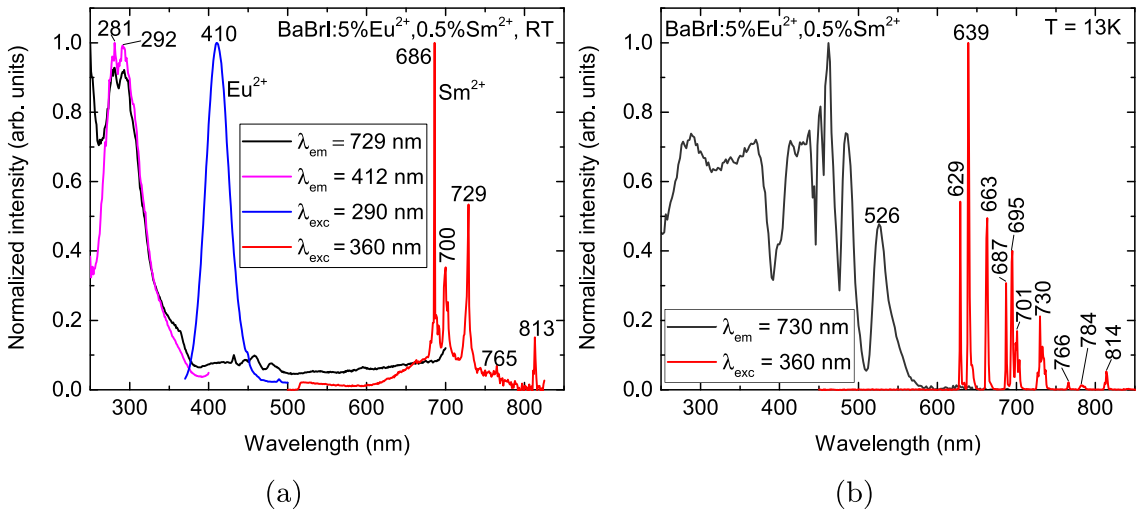

Fig. 3. Emission and excitation spectra of BaBrI:5%Eu^{2+},0.5%Sm^{2+} measured with a Horiba Scientific QuantaMaster fluorometer a) at room temperature and b) with a Newport 66921 xenon lamp in combination with a Horiba Gemini 180 and a Princeton Instruments Acton SP 2300 excitation and emission monochromators, and detected with a Hamamatsu R7600U-20 PMT at 13 K. Emission spectra in a) are corrected for the monochromator and detector efficiencies.

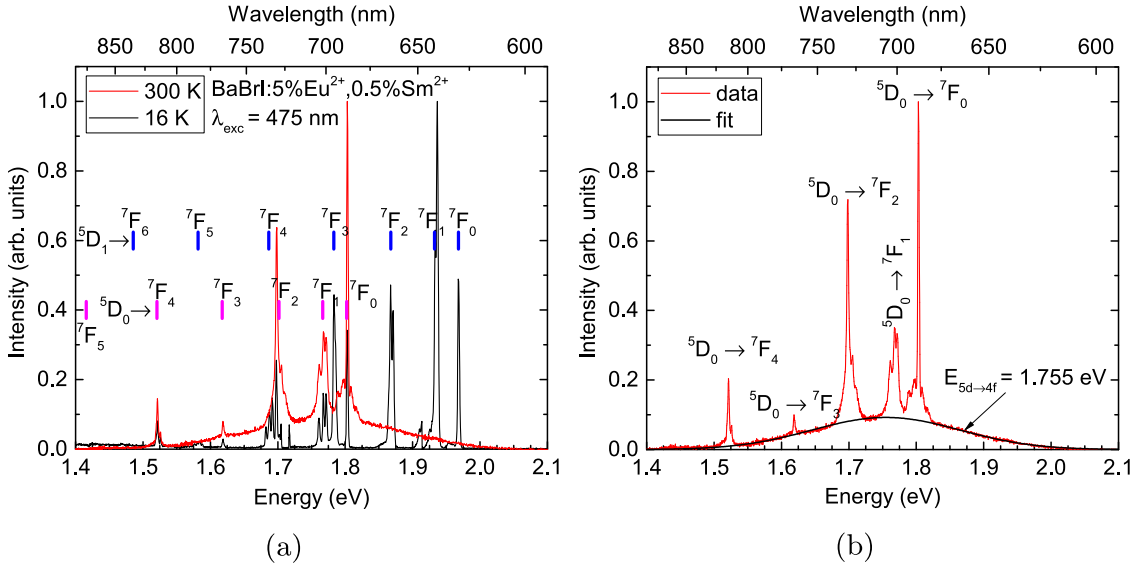

Fig. 4. a.) Emission spectrum of BaBrI:5%Eu^{2+},0.5%Sm^{2+} excited at 475 nm with an OPO laser at 16 K and 300 K. Vertical lines show 4f-4f transition energies of Sm^{2+} ion in BaClF measured by Kiss and Weakliem [20] b.) Gaussian fit of the Sm^{2+} 5d→4f emission peak under the 4f→4f lines observed at 300 K. The spectra are not corrected for the monochromator and detector efficiencies.

chosen to estimate the degree of spectral overlap between excitation and emission of Sm^{2+} and provide some clue if Sm^{2+} might have lower spectral overlap than Eu^{2+}. Europium emission is observed at 410 nm and can be excited with 290 nm light at room temperature. The room temperature excitation spectrum of samarium (λ_{em} = 729 nm) shown in Fig. 3a has a characteristic peak at 292 nm in coincidence with the europium excitation spectrum. This is a direct proof of energy transfer from europium to samarium. Wavelengths from 400 to 600 nm directly excite Sm^{2+}, while below 400 nm both Sm^{2+} and Eu^{2+} are excited followed by Eu^{2+} to Sm^{2+} energy transfer. Interestingly,the samarium emission intensity is much lower for direct excitation (400–600 nm) than for europium excitation (292 nm) and subsequent energy transfer. This is due to the 10 times lower samarium concentration in the crystal which results in weak samarium absorption. Since Sm^{2+} concentration is low, the Sm^{2+} excitation spectrum is strongly affected by a high background from the monochromator stray light. This results in an artificial increase of excitation intensity above 600 nm.

Fig. 3b depicts a significant change of the samarium emission in BaBrI:5%Eu^{2+},0.5%Sm^{2+} at 13 K. The broad 5d→4f emission at ~700 nm disappears, and five new sharp lines appear. The excitation spectrum is much better resolved at 13 K (Fig. 3b) than at room temperature (Fig. 3a) and shows a series of Sm^{2+} 4f→5d excitation bands between 400 and 600 nm. The direct excitation of Sm^{2+} seems to increase at low temperature as compared to the Eu^{2+} excitation intensity, but it is rather an instrumental artifact caused by increased emission intensity of both dopants together with saturation of the Eu^{2+} excitation band at 292 nm. The lowest excitation peak of Sm^{2+} becomes visible at 526 nm, and an additional shoulder at around 540 nm appears. These two excitation bands are usually referred to as samarium A and B bands [19], in this case at 540 nm and 526 nm, correspondingly.

Fig. 4a shows BaBrI:Eu^{2+},Sm^{2+} emission spectra at 16 K and 300 K. Vertical lines indicate 4f→4f Sm^{2+} transition energies measured in BaClF:Sm^{2+} by Kiss and Weakliem [20]. A good match is observed between 4f→4f transition energies in both compounds, and it illustrates a

Table 1
Energies of Sm^{2+} 4f-4f emission transitions in BaBrI:5%Eu^{2+},0.5%Sm^{2+}.

Excited state	Ground state	Wavelength (nm)	Energy (eV)
$^5D_0$	$^7F_0$	687	1.805
	$^7F_1$	702	1.766
	$^7F_2$	730	1.699
	$^7F_3$	767	1.617
	$^7F_4$	815	1.521
$^5D_1$	$^7F_0$	629	1.971
	$^7F_1$	640	1.938
	$^7F_2$	663	1.870
	$^7F_3$	695	1.784
	$^7F_4$	733	1.692
	$^7F_5$	784	1.582

low sensitivity of 4f→4f transition energies on the host environment. The $^5D_0 \rightarrow {}^7F_J$ transitions with $J = 0$–4 can be easily identified as dominating at room temperature. The strongest line at 1.804 eV (687 nm) is the $^5D_0 \rightarrow {}^7F_0$ transition. $^5D_0 \rightarrow {}^7F_J$ emissions with $J = 0$–5 arise at low temperature and become dominating. No emission to the $^7F_6$ state is observed. The broad 5d→4f band is absent at 16 K. We conclude that BaBrI:Eu^{2+},Sm^{2+} adopts the situation shown in Fig. b). Table 1 summarizes the wavelengths and energies of the observed 4f→4f transitions. Fig. 4b shows the room temperature emission spectrum with a Gaussian fit to the 5d-4f peak. The band center is at 1.755 eV which corresponds to 707 nm.

Fig. 5a shows photoluminescence emission and excitation spectra of $CsBa_2I_5$:2%Eu^{2+},1%Sm^{2+} at room temperature. Both dopants, Eu^{2+} and Sm^{2+} are characterized by single emission peaks observed at 423 nm and 762 nm, respectively. The excitation spectrum of Eu^{2+} is characterized by two excitation peaks at 290 nm and 333 nm. These peaks coincide with the Sm^{2+} excitation spectrum and indicate energy transfer from europium to samarium. The Sm^{2+} excitation spectrum shows additional peaks for direct excitation with the lowest peak at 613 nm.

Fig. 5b shows excitation and emission spectra of Sm^{2+} and Eu^{2+} ions in a $CsSrI_3$:%2Eu^{2+},1%Sm^{2+} at room temperature. The Sm^{2+} emission spectrum in $CsSrI_3$ is not shown here because it was outside the sensitive range of the QuantaMaster fluorometer. This spectrum was already presented in Fig. 2 measured with a CCD detector and a home-made PL/PLE spectrometer described in the methods section. The Eu^{2+} photoluminescence is characterized by a single peak at 456 nm. The excitation

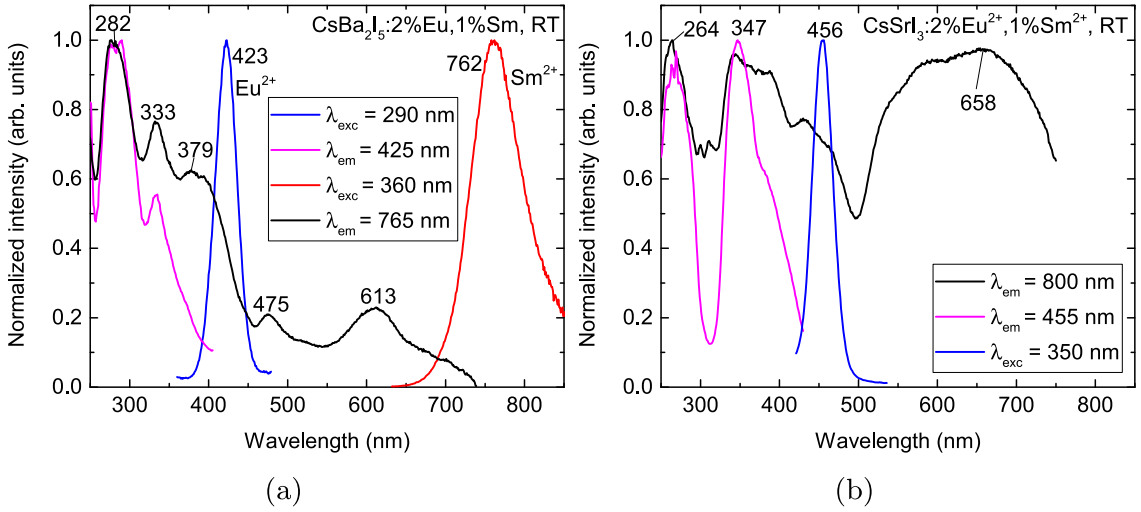

Fig. 5. Photoluminescence emission and excitation spectra of Eu^{2+} and Sm^{2+} ions in a) $CsBa_2I_5$:2%Eu^{2+},1%Sm^{2+} and b) $CsSrI_3$:2%Eu^{2+},1%Sm^{2+} measured with a Horiba Scientific QuantaMaster fluorometer at room temperature. The spectra are corrected for the monochromator and detector efficiencies.

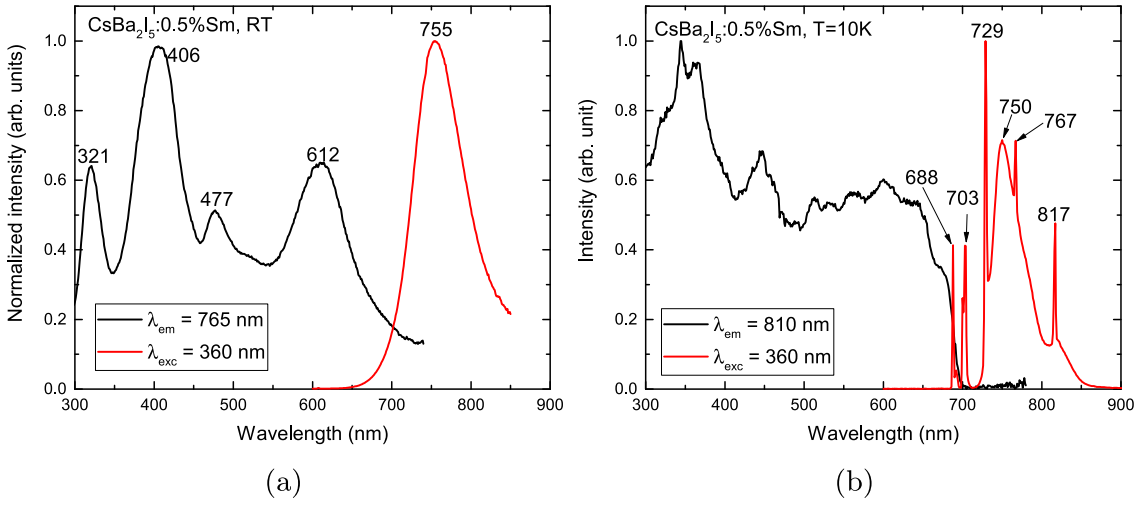

Fig. 6. Photoluminescence emission and excitation spectra of $CsBa_2I_5$:0.5%Sm^{2+} a) at room temperature measured with a Horiba Scientific QuantaMaster fluorometer and b) at 10 K measured with a xenon lamp excitation and a Hamamatsu R7600U-20 photomultiplier. The emission spectrum in Fig. a) is corrected for the monochromator and detector efficiencies.

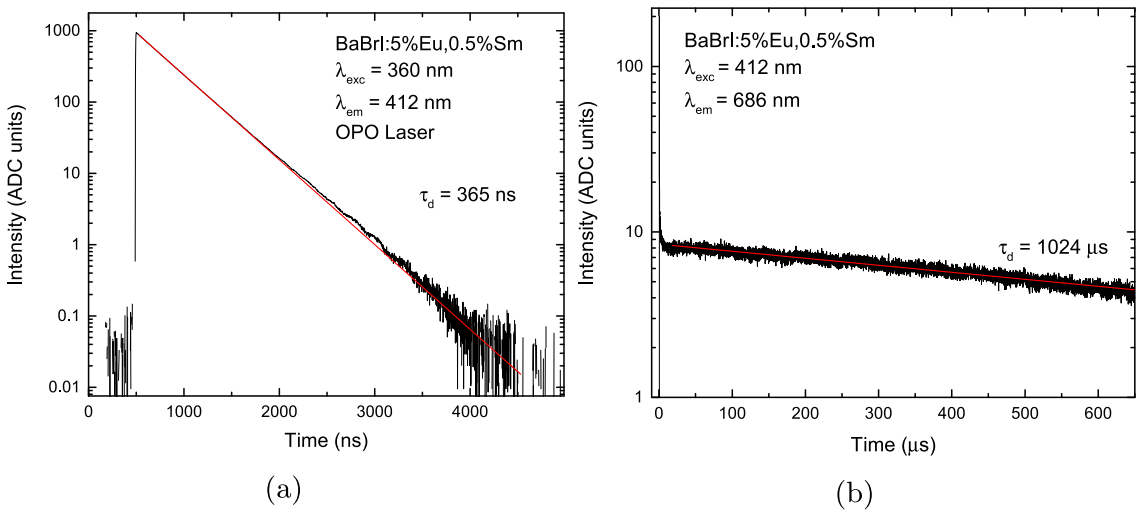

Fig. 7. a.) Photoluminescence decay profile of BaBrI:5%Eu^{2+},0.5%Sm^{2+} at room temperature) 360 nm photoluminescence excitation and emission observed at 412 nm (Eu^{2+} 4f-5d transition). b) 412 nm photoluminescence excitation and emission observed at 686 nm (Sm^{2+} $^5D \rightarrow 0^7F_0$ transition).

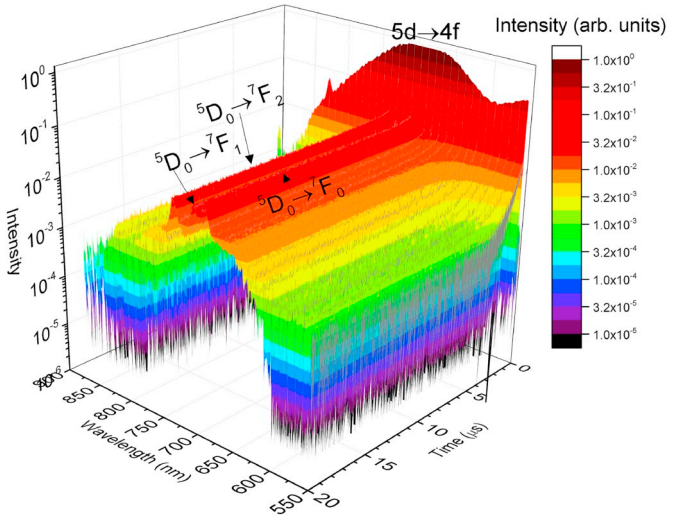

Fig. 8. Time-resolved photoluminescence of BaBrI:5%Eu^{2+},0.5%Sm^{2+} at room temperature excited at 410 nm with an OPO laser. The spectrum is not corrected for the monochromator and detector efficiencies.

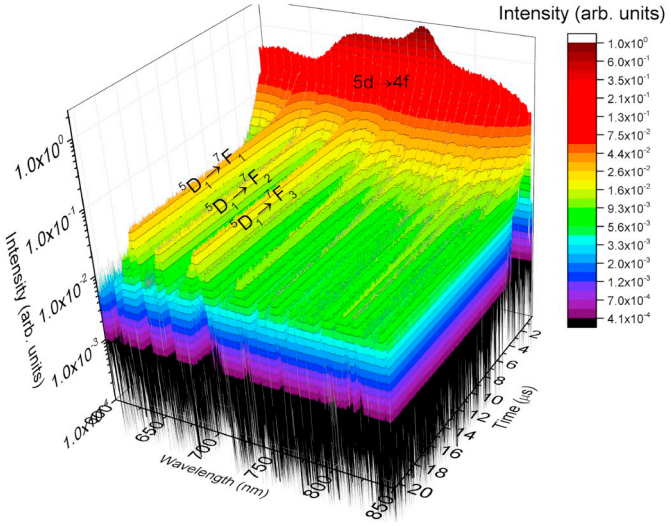

Fig. 9. Time resolved photoluminescence of BaBrI:5%Eu^{2+},0.5%Sm^{2+} at 11 K excited at 360 nm with an OPO laser. The spectrum is not corrected for the monochromator and detector efficiencies.

spectrum of Eu^{2+} shows two peaks at 264 nm and 347 nm. These two excitation peaks are in coincidence with Sm^{2+} excitation peaks and indicate Eu→2+Sm^{2+} energy transfer. The lowest energy (direct) excitation peak of Sm^{2+} is at 658 nm.

Fig. 6 shows excitation and emission spectra of Sm^{2+} ions in $CsBa_2I_5$:0.5%Sm^{2+} at room temperature and 10 K. The emission spectrum is identical to that of $CsBa_2I_5$:2%Eu^{2+},1%Sm^{2+} (Fig. 5a), with an obvious lack of the Eu^{2+} peak. The excitation spectrum measured at room temperature (Fig. 6a) has multiple Sm^{2+} excitation bands extending from 300 nm to 750 nm. The lowest excitation band at 612 nm corresponds to the same excitation peak observed in $CsBa_2I_5$:2% Eu^{2+},1%Sm^{2+} at room temperature, see Fig. 5a The emission spectrum of Sm^{2+} changes dramatically at 10 K. Five sharp emission lines appear that can be identified as 4f-4f transitions from the $^5D_0$ Sm^{2+} state to the $^7F_0$ (688 nm), $^7F_1$ (703 nm), $^7F_2$ (729 nm), $^7F_3$ (767 nm), and $^7F_4$ (817 nm) states. The d-f emission peak is observed at 750 nm. The peak width is narrower at 10 K and reveals a shoulder at ~825 nm.

4.2. Time-resolved measurements

Sm^{2+} emission in $CsBa_2I_5$:2%Eu^{2+},1%Sm^{2+} and $CsSrI_3$:2%Eu^{2+},1% Sm^{2+} at room temperature is only of 5d-4f type with a single decay constant. For the time resolved measurement we focused on BaBrI:5% Eu^{2+},0.5%Sm^{2+} because, different from the other two compositions, here we deal with a competition between 4f-4f and 4f-5d emission.

Fig. 7a shows photoluminescence decay profile of the Eu^{2+} ion in BaBrI:5%Eu^{2+},0.5%Sm^{2+}; a single-exponential fit yields a decay time of 365 ns. Fig. 7b shows the Sm^{2+} photoluminescence decay of the $^5D \rightarrow 0^7F_0$ transition at 686 nm. Its single-exponential decay time of 1024 µs is too long for most scintillator applications. A fast decay is observed at the leading edge of Sm^{2+} emission in Fig. 7b It originates from the 5d→4f emission band which has a fast decay time of 14 ns and overlaps with all 4f→4f lines. The short decay time is due to the fast depopulation of the 4f5d state to the lower energy $^5D_0$ state.

Fig. 8 shows the time-resolved photoluminescence of BaBrI:Eu^{2+}, Sm^{2+} at room temperature. It is characterized at time zero by a broad band arising from the 14 ns fast 5d→4f Sm^{2+} emission and followed by

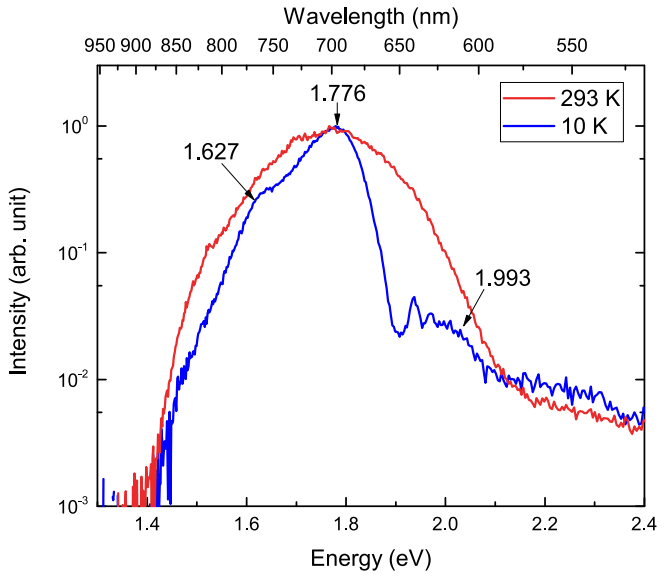

Fig. 10. Time-gated OPO laser excited emission of Sm^{2+} at 10 K and room temperature. Excitation at 412 nm and a 100 ns gate were used. The spectra are not corrected for the monochromator and detector efficiencies.

the 1024 μs slow 4f→4f line emissions. The line emissions are located on top of a Gaussian shape emission long time after the initial fast 5d→4f emission has decayed. This suggest thermal re-population of the emitting 4f5d state from the lower energy $^5D_0$ state. The situation changes significantly at 11 K in Fig. 9, when the 5d→4f emission is observed after the excitation at time zero, and it completely decays within 2 μs? Apparently, thermal re-population of the 4f5d state is impossible at 11 K, so only initially excited 5d→4f emission is detected.

Fig. 10 shows time-gated emission spectra of Sm^{2+} at room temperatures and 10 K. A short 100 ns gate eliminates the slow 4f→4f emission from the emission spectrum, and only fast 5d→4f emission is observed. The peak at room temperature is very broad, and has no structure. Measurement at 10 K reveals structure in the band, and subbands at 1.627, 1.76, and 1.993 eV can be distinguished. This suggests that multiple 4f final state levels are involved in 5d→4f emission resulting in a multi-peak structure of the emission spectrum.

4.3. Temperature resolved measurements

Fig. 11a shows the change of the Sm^{2+} emission in BaBrI:5% Eu^{2+},0.5%Sm^{2+} as a function of temperature. Intensity of 4f-4f transitions decreases with increasing temperature, while at high temperature a broad 5d-4f emission band becomes dominating. New emission lines are observed at around 100 K and below. These are ascribed to $^5D \rightarrow 1^7F_J$ transitions.

Fig. 11b shows the total integrated intensity of the Sm^{2+} emission spectrum in BaBrI:5%Eu^{2+},0.5%Sm^{2+}. At 50 K emissions are dominated by $^5D \rightarrow 0^7F_J$ transitions with addition of $^5D \rightarrow 1^7F_J$ transitions. The intensity of $^5D \rightarrow 1^7F_J$ transitions decreases quickly with increasing temperature, and these transitions are not detectable above 100 K. The 5d-4f emission becomes visible at around 200 K, and its intensity increases with temperature. 5d-4f emission becomes dominating above 400 K.

5. Discussion

Optical spectra in Figs. 3 and 5 show overlap of Eu^{2+} and Sm^{2+} excitation proving the presence of Eu→2+Sm^{2+} energy transfer. It is very clearly seen in the BaBrI:5%Eu^{2+},0.5%Sm^{2+} sample, where due to

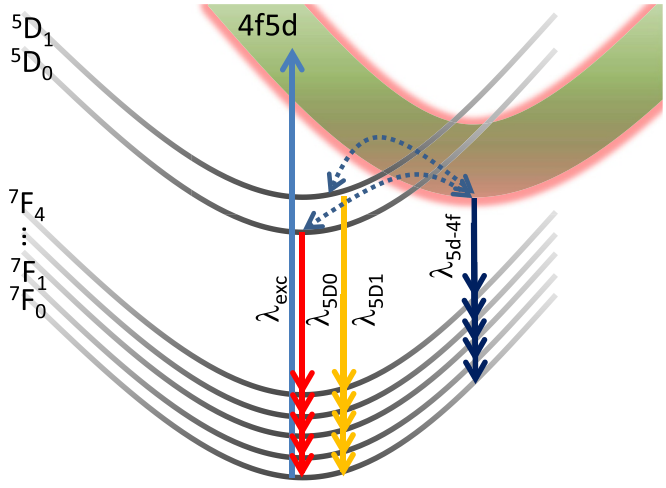

Fig. 12. Configurational coordinate diagram of Sm^{2+} in BaBrI. Solid arrows indicate radiative, dotted arrows non-radiative processes.

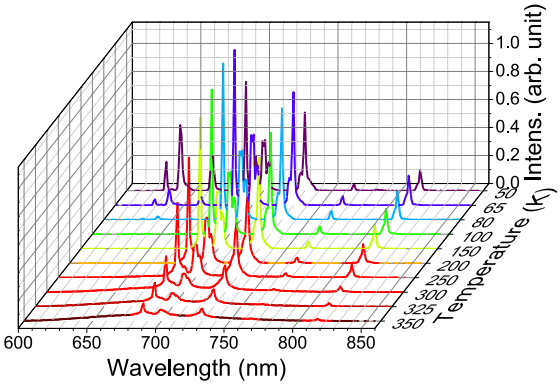

(a)

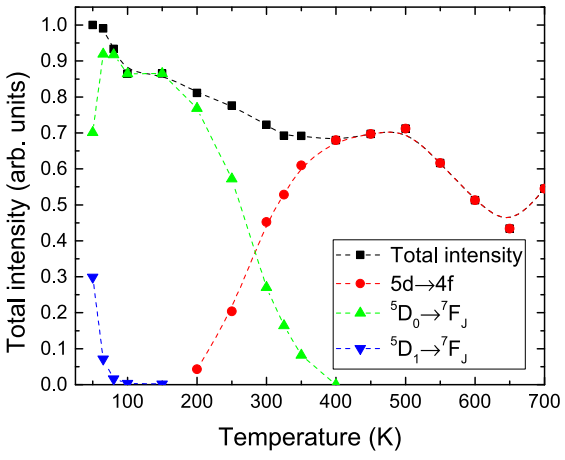

(b)

Fig. 11. a.) Photoluminescence emission spectrum of Sm^{2+} in BaBrI:5%Eu^{2+},0.5%Sm^{2+} versus temperature using 360 nm photoluminescence excitation b.) Intensity of different Sm^{2+} transitions in BaBrI:5%Eu^{2+},0.5%Sm^{2+} versus temperature using 360 nm photoluminescence excitation.

low Sm^{2+} concentration the direct excitation of Sm^{2+} (400–600 nm) is around 10 times weaker than excitation of europium (292 nm) with the following energy transfer Eu→2+Sm^{2+}.

A shift of the lowest excitation energy band of Eu^{2+} is observed from 292 nm in BaBrI (Fig. 3a) to 333 nm in $CsBa_2I_5$ (Figs. 5a) and 347 nm in $CsSrI_3$ (Fig. 5b). Sm^{2+} shows a similar trend with the lowest excitation energy at 526 nm in BaBrI (Fig. 3b at 13 K), 613 nm in $CsBa_2I_5$ (Figs. 5a), and 658 nm in $CsSrI_3$ (Fig. 5b). This shift of the lowest 5d energy level of Eu^{2+} and Sm^{2+} is related to the crystal field splitting in the different host crystals which strongly affects the d- and only marginally the f-states [21]. A detailed discussion of Eu^{2+} emission and absorption shift with change of host lattice, the coordination number of the cations, the anionic–Eu bond lengths, the symmetry, and the so-called nephelauxetic effect can be found in Ref. [22].

Fig. 12 shows a configurational coordinate diagram for Sm^{2+} in BaBrI which explains the changes of the emission spectra with temperature observed in Figs. 8 and 9. At 13 K, 4f→5d excitation is followed by non-radiative relaxation to $^5D_0$ and $^5D_1$ states, and 5d→4f emission is observed only shortly after the excitation. Thermally activated transitions back to the 4f5d state are impossible. As temperature rises the excited 4f5d state becomes thermally populated from the $^5D_0$ and $^5D_1$ states, and both types of luminescent transitions are observable at room temperature. The $^5D_1$ emission disappears at room temperature, which can be explained either by ionization to the conduction band or thermally-activated transition from $^5D_1$ back to the 4f5d state.

The situation is different in the $CsBa_2I_5$ host. Fig. 6 shows that Sm^{2+} has only 5d-4f emission at room temperature. The 4f-4f emission appears below 100 K, but the 5d-4f emission is not completely gone even at 10 K. This is an indication that the bottom of 4f5d state of Sm^{2+} in $CsBa_2I_5$ is below the $^5D_0$ state. This ensures that at room temperature the allowed 5d-4f emission dominates, and we deal with the preferred level location as initially presented in Fig. a.

Fig. 10 shows that the time-gated Sm^{2+} emission spectrum in BaBrI measured at 10 K has a structure which is not visible at room temperature. There are three peaks visible, and a shoulder at 2.3 eV extending to higher energies. Similar three-peak emission structure was observed in other Sm^{2+}-doped materials [23] and interpreted as de-excitations from the 4f5d level to the $^7F_0$, $^7F_1$, and $^7F_2$ final states [24]. However, the energy spacing between the sub-bands in Fig. 10 does not match the energy spacing between the $^7F_{0-2}$ final levels (Table 1).

In contrary to previous research on BaBrI:Eu by Shalaev et al. [25], we observed thermal quenching of Eu^{2+} and Sm^{2+} emission BaBrI:5% Eu^{2+},0.5%Sm^{2+} at much higher temperature. They have measured that Eu^{2+} luminescence intensity decreases by 50% at 365 K (when compared to 200 K) in BaBrI:Eu (0.05% Eu), while our sample shows 50% decrease of luminescence intensity at 700 K. This difference can be caused by different excitation wavelength used for measuring of emission spectrum (295 nm in Shalaev et al., 360 nm in this work), different europium concentration (0.05% Eu^{2+} in Shalaev et al., 5% Eu^{2+} in this work), or addition of Sm^{2+} has positive influence on quenching characteristic of this material. This effect requires a dedicated effort to be understood. A shorter decay time of Shalaev's sample might indicate that the sample's purity/quality may be a serious issue.

To obtain the preferred 5d→4f emission for scintillation application we have to make sure that the lowest energy 4f5d level is at similar or lower energy than the $^5D_0$ excited state. It is known that the 4f5d level red-shifts towards lower energies with change of anion of the host according to the nephelauxetic sequence:

$$F^- < Cl^- < Br^- < I^-$$

Iodides are the most promising hosts for obtaining 5d→4f emission of the Sm^{2+} dopant. We can provide a much stronger and practical requirement based on systematics in lanthanides spectroscopy.

Since there are much more data on Eu^{2+} emission energy $E_{Eu^{2+}}$, we can use lanthanide phenomenology to predict Sm^{2+} emission. Dorenbos showed that the 4f5d level energy of divalent lanthanides is linearly correlated [21]. The energy of Sm^{2+} 5d→4f emission can be written as:

$$E_{Sm^{2+}} = E_{Eu^{2+}} - 1.22 \text{ eV}. \quad (1)$$

Since the $^5D_0$ level is located at 1.805 eV, we can state a criterion for 5d→4f emission as follows: $E_{Sm^{2+}} < 1.805$ eV. If we include 25 meV margin for thermal excitation it results in a requirement that europium emission energy must be lower than 2.995 eV or

$$\lambda^{em.}_{Eu^{2+}} > 414 \text{ nm}. \quad (2)$$

On basis of this requirement we propose in Table 2 suitable candidate scintillators for applying the Eu→2+Sm^{2+} energy transfer mechanism. We selected europium doped materials with known high light yield and high energy resolution, and calculated the expected Sm^{2+} emission wavelengths using Eq. (1). These values agree well with measured photoluminescence Sm^{2+} 5d→4f emissions in $CsBa_2I_5$ (Fig. 2), SrI_2 [26], BaBrI (4b), and $CsSrI_3$ (Fig. 2).

We conclude that many recently developed europium doped scintillators ($KCaI_3$:Eu, KSr_2I_5:Eu etc.) can be used as well with Sm^{2+} doping. Also, the recently discovered thallium-based scintillators can provide the allowed 5d-4f emission of samarium. According to our predictions, all these materials can be turned into red or near-red scintillator by using samarium co-doping.

Table 2
Candidate scintillators for applying the Eu→2+Sm^{2+} energy transfer mechanism for NIR scintillation. L.Y. – light yield of Eu^{2+} doped material at 662 keV of γ-photon excitation, R – energy resolution at 662 keV, $\tau_{Eu^{2+}}$ – decay time of the most intense component of Eu^{2+} scintillation, $\lambda^{em.}_{Sm^{2+}}$ – – 5d-4f Sm^{2+} emission predicted/measured.

Compound	L.Y. (kPh/MeV)	R (% FWHM)	$\tau_{Eu^{2+}}$ (ns)	$\lambda^{em.}_{Eu^{2+}}$ (nm)	Ref. Eu^{2+}	$\lambda^{em.}_{Sm^{2+}}$ pred. (nm)	$\lambda^{em.}_{Sm^{2+}}$ meas. (nm)
BaBrI:Eu	97	3.4	432	413	[12]	696	701 (this work)
SrI_2:Eu	100	2.6	1000	431	[11]	748	753 [15, 26]
$CsBa_2I_5$:Eu	80–102	2.3–2.55	1000	432	[12, 13]	751	758 (this work & [16])
$CsSrI_3$	65	5.9	3300	454	[27]	820	839 (this work)
$KCaI_3$:Eu	72	3.0	1060	466	[28]	861	–
KSr_2I_5:Eu	94	2.4	990	445	[29]	792	–
K_2BaI_4:Eu	57	2.7	720	448	[29]	801	–
KSr_2Br_5:Eu	75	3.5	1080	427	[29]	736	–
KBa_2I_5:Eu	87	2.6	910	444	[29]	788	–
$TlSr_2I_5$:Eu	79	4.2	525	463	[30]	850	–

6. Conclusions

Co-doping with samarium has been shown to be an effective way of shifting emission of europium in halide scintillators. All three studied samples, BaBrI:5%Eu^{2+},0.5%Sm^{2+}, $CsBa_2I_5$:2%Eu^{2+},1%Sm^{2+}, and $CsSrI_3$:%2Eu^{2+},1%Sm^{2+} show energy transfer from Eu^{2+} to Sm^{2+} under optical excitation. In $CsBa_2I_5$ and $CsSrI_3$ samarium shows single 5d-4f emission peak, while BaBrI is a "border-case" host in which Sm^{2+} ions shows both 5d→4f and 4f→4f emission. 1 ms day time of 4f→4f emission makes a scintillation pulse height spectrum measurement virtually impossible, and BaBrI:5%Eu^{2+},0.5%Sm^{2+} can not be used as a scintillator in γ-ray spectroscopy at room temperature. Interestingly, the 4f-4f emission disappears above 400 K and offers a possibility of using BaBrI:5%Eu^{2+},0.5%Sm^{2+} as a high temperature scintillator. Although it may not find application in standard γ spectroscopy, it still may be used

e.g. as a red-emitting X-ray phosphor or luminescence thermometer [31, 32].

$CsBa_2I_5:Eu^{2+},Sm^{2+}$ and $CsSrI_3:Eu^{2+},Sm^{2+}$ both offer allowed 5d-4f transitions at room temperature, and both materials have suitable optical properties for scintillation detection.

Acknowledgments

This work was supported by the Dutch Technology Foundation STW, which is part of the Netherlands Organization for Scientific Research (NWO), which is partly funded by the Ministry of Economic Affairs. This work was partly funded by Saint Gobain Crystals, France.

Appendix A. Supplementary data

Supplementary data to this article can be found online at https://doi.org/10.1016/j.jlumin.2020.117101.

Author statement

W. Wolszczak: Investigation, Formal analysis, Writing - original draft, Visualization, P. Dorenbos: Supervision, Writing - review & editing, K. Krämer: Resources, Writing - review & editing

References

[1] P.A. Rodnyi, Physical Processes in Inorganic Scintillators, vol. 14, CRC press, 1997.
[2] G.F. Knoll, Radiation Detection and Measurement, John Wiley & Sons, 2010.
[3] P. Lecoq, A. Gektin, M. Korzhik, Inorganic Scintillators for Detector Systems: Physical Principles and Crystal Engineering, Springer, 2016.
[4] P. Lecoq, Development of new scintillators for medical applications, Nucl. Instrum. Methods Phys. Res. Sect. A Accel. Spectrom. Detect. Assoc. Equip. 809 (2016) 130–139. Advances in detectors and applications for medicine.
[5] J. Glodo, Y. Wang, R. Shawgo, C. Brecher, R.H. Hawrami, J. Tower, K.S. Shah, New developments in scintillators for security applications, Physics Procedia, in: Conference on the Application of Accelerators in Research and Industry, CAARI 2016, 30 October – 4 November 2016, Ft, vol. 90, 2017, pp. 285–290. Worth, TX, USA.
[6] I. Mitrofanov, A. Kozyrev, A. Konovalov, M. Litvak, A. Malakhov, M. Mokrousov, A. Sanin, V. Tret'ykov, A. Vostrukhin, Y. Bobrovnitskij, T. Tomilina, L. Gurvits, A. Owens, The mercury gamma and neutron spectrometer (MGNS) on board the planetary orbiter of the BepiColombo mission, Planet. Space Sci. 58 (1) (2010) 116–124. Comprehensive Science Investigations of Mercury: The scientific goals of the joint ESA/JAXA mission BepiColombo.
[7] C.C. Hansson, A. Owens, J.v.d. Biezen, X-ray, γ-ray and neutron detector development for future space instrumentation, Acta Astronaut. 93 (2014) 121–128.
[8] A. Kozyrev, I. Mitrofanov, A. Owens, F. Quarati, J. Benkhoff, B. Bakhtin, F. Fedosov, D. Golovin, M. Litvak, A. Malakhov, M. Mokrousov, I. Nuzhdin, A. Sanin, V. Tretyakov, A. Vostrukhin, G. Timoshenko, V. Shvetsov, C. Granja, T. Slavicek, S. Pospisil, A comparative study of $LaBr^3(Ce^{3+})$ and $CeBr^3$ based gamma-ray spectrometers for planetary remote sensing applications, Rev. Sci. Instrum. 87 (8) (2016), 085112.
[9] P. Lecoq, The high energy physics demand for a new generation of scintillators, J. Lumin. 60–61 (1994) 948–955.
[10] R. Mao, L. Zhang, R. Zhu, Optical and scintillation properties of inorganic scintillators in high energy physics, IEEE Trans. Nucl. Sci. 55 (Aug 2008) 2425–2431.
[11] M.S. Alekhin, J.T.M. de Haas, K.W. Krämer, I.V. Khodyuk, L. de Vries, P. Dorenbos, Scintillation properties and self absorption in $SrI^2:Eu^{2+}$,, in: IEEE Nuclear Science Symposuim Medical Imaging Conference, Oct 2010, pp. 1589–1599.
[12] G. Bizarri, E.D. Bourret-Courchesne, Z. Yan, S.E. Derenzo, Scintillation and optical properties of $BaBrI:Eu^{2+}$ and $CsBa^2I^5:Eu^{2+}$, IEEE Trans. Nucl. Sci. 58 (Dec 2011) 3403–3410.
[13] M.S. Alekhin, D.A. Biner, K.W. Krämer, P. Dorenbos, Optical and scintillation properties of $CsBa^2I^5:Eu^{2+}$, J. Lumin. 145 (2014) 723–728.
[14] C. Dujardin, E. Auffray, E. Bourret-Courchesne, P. Dorenbos, P. Lecoq, M. Nikl, A. N. Vasil'ev, A. Yoshikawa, R.Y. Zhu, Needs, trends, and advances in inorganic scintillators, IEEE Trans. Nucl. Sci. 65 (Aug 2018) 1977–1997.
[15] R. Awater, M. Alekhin, D. Biner, K. Krämer, P. Dorenbos, Converting $SrI^2:Eu^{2+}$ into a near infrared scintillator by Sm^{2+} co-doping, J. Lumin. 212 (2019) 1–4.
[16] W. Wolszczak, K.W. Krämer, P. Dorenbos, $CsBa^2I^5:Eu^{2+},Sm^{2+}$ – the first high-energy resolution black scintillator for γ-ray spectroscopy, Phys. Status Solidi Rapid Res. Lett. (2019) 1900158.
[17] W. Döll, W. Klemm, Messungen an zwei-und vierwertigen Verbindungen der seltenen Erden. VII. Über die Struktur einiger Dihalogenide, Z. Anorg. Allg. Chem. 241 (2–3) (1939) 239–258.
[18] G. Schilling, G. Meyer, Ternäre Bromide und Iodide zweiwertiger Lanthanide und ihre Erdalkali-Analoga vom Typ AMX^3 und AM^2X^5, Z. Anorg. Allg. Chem. 622 (5) (1996) 759–765.
[19] D. Wood, W. Kaiser, Absorption and fluorescence of Sm^{2+} in CaF^2, SrF^2, and BaF^2, Phys. Rev. 126 (6) (1962) 2079.
[20] Z. Kiss, H. Weakliem, Stark effect of 4 states and linear crystal field in $BaClF:Sm^{2+}$, Phys. Rev. Lett. 15 (10) (1965) 457.
[21] P. Dorenbos, f →d transition energies of divalent lanthanides in inorganic compounds, J. *Phys. Condens. Matter* 15 (jan 2003) 575–594.
[22] P. Dorenbos, Energy of the first $4f^7 \rightarrow 4f^65d$ transition of Eu^{2+} in inorganic compounds, J. Lumin. 104 (4) (2003) 239–260.
[23] M. Karbowiak, P. Solarz, R. Lisiecki, W. Ryba-Romanowski, Optical spectra and excited state relaxation dynamics of Sm^{2+} ions in $SrCl^2$, $SrBr^2$ and SrI^2 crystals, J. Lumin. 195 (2018) 159–165.
[24] P. Larsen, Lumineszenz zweiwertiger Selten-Erd-Ionen in Bromidischen Wirtsgittern, PhD thesis, Universität zu Köln, 2004.
[25] A. Shalaev, R. Shendrik, A. Myasnikova, A. Bogdanov, A. Rusakov, A. Vasilkovskyi, Luminescence of BaBrI and SrBrI single crystals doped with Eu^{2+}, Opt. Mater. 79 (2018) 84–89.
[26] M.S. Alekhin, R.H. Awater, D.A. Biner, K.W. Krämer, J.T. de Haas, P. Dorenbos, Luminescence and spectroscopic properties of Sm^{2+} and Er^{3+} doped SrI^2, J. Lumin. 167 (2015) 347–351.
[27] K. Yang, M. Zhuravleva, C.L. Melcher, Crystal growth and characterization of $CsSr^{1-x}Eu_xI^3$ high light yield scintillators, Phys. Status Solidi Rapid Res. Lett. 5 (1) (2011) 43–45.
[28] A.C. Lindsey, M. Zhuravleva, L. Stand, Y. Wu, C.L. Melcher, Crystal growth and characterization of europium doped $KCaI^3$, a high light yield scintillator, Opt. Mater. 48 (2015) 1–6.
[29] L.M. Stand Stracuzzi, Discovery and Development of Potassium-Based Metal Halide Scintillators for Radiation Detection Applications, PhD thesis, University of Tennessee, Knoxville, 2018.
[30] H. Kim, G. Rooh, A. Khan, H. Park, S. Kim, Scintillation performance of the $TlSr^2I^5(Eu^{2+})$ single crystal, Opt. Mater. 82 (2018) 7–10.
[31] M. Dramicanin, Luminescence Thermometry: Methods, Materials, and Applications, Elsevier, April 2018.
[32] C.D.S. Brites, S. Balabhadra, L.D. Carlos, Lanthanide-based thermometers: at the cutting-edge of luminescence thermometry, Advanced Optical Materials 7 (5) (2019) 1801239.